PCCP

Computer simulation of water molecules at kaolinite and silica surfaces

M. R. Warne,* N. L. Allan and T. Cosgrove

School of Chemistry, University of Bristol, Cantock's Close, Bristol, UK BS8 1TS.
E-mail: mark.warne@bristol.ac.uk

Received 18th May 2000, Accepted 20th June 2000
Published on the Web 25th July 2000

Molecular dynamics simulations of water molecules at the surface of kaolinite, and of amorphous silica, have been carried out. In contrast to previous work, clay and silica atoms are *not* kept fixed at their crystallographic positions; all atoms are allowed to move. In both cases water molecules at the surface show a marked decrease in the self-diffusion coefficient and an increase in the rotational correlation time. We consider the effects of increasing the ionic strength of the water. Comparison with experimental data is made by linking calculated diffusion and rotational correlation times to available pulse field gradient nuclear magnetic resonance spectroscopy and relaxation measurements.

1 Introduction

The molecular structure and dynamics of interfaces between inorganic solids and liquids are of particular interest because of the influence they exert on the stabilisation properties of colloidal systems. The behaviour of water–clay systems, for example, is important since interlayer water acts as a solvent for intercalated species. Clays are abundant natural decomposition products of aluminosilicates in aqueous environments, and an understanding of the factors at the atomic level that control the orientation, translation and rotation of water molecules at the mineral surface has implications for processes such as the preparation of pigment dispersions used in paper coatings.

Various simulation techniques have been used previously to investigate clay–water systems.[1–19] All these models either keep the clay structure rigid, or allow unrealistic movements of Al and Si atoms at the clay surface. Keeping the clay rigid may be appropriate when considering the effects of water on interlayer distance during clay swelling, but relaxation of the hydroxy groups and other surface atoms might be crucial in the molecular adsorption process and in determining the dynamic behaviour of water molecules at the interface.

Fig. 1 shows the crystal structure of kaolinite (two unit cells). The kaolin mineral consists of 1 : 1 dioctahedral layers with overall chemical composition $Si_2Al_2O_5(OH)_4$. The framework structure is composed of a sheet of vertex-sharing SiO_4 tetrahedra, linked by common oxygen atoms parallel to the *c*-axis to a sheet of edge-sharing AlO_6 octahedra. It is important to note that this is an idealised structure since disorder is common in kaolin minerals, and together with the small particle size leads to complications in structure elucidation. The kaolinite structure used here was that determined experimentally by Bish and Von Dreele.[20] However, these authors do not report the positions of the hydrogen atoms, about which there is no general agreement.[21,22] We have combined their heavy-atom positions with the hydrogen positions used in the periodic Hartree–Fock calculations of Hess and Saunders,[23] which produces a structure with C_1 symmetry.

In this work we build on earlier static simulations of trace elements in the bulk and the {001} surface of muscovite[24] to carry out molecular dynamics of the water–clay system using an atomistic model of the clay in which atoms are *not* kept fixed at their crystallographic positions. We have compared the behaviour of water at the kaolinite surface with that at the surface of amorphous silica, using the same intermolecular potential model for the amorphous silica as for the kaolinite and again allowing all atoms to move. The arrangement of the OH groups at the surface of kaolinite is much more regular than that at the silica surface. The effects of changing the ionic strength of the water are also considered in both cases. We have examined the spatial motion distribution functions of water molecules away from the mineral surface and their diffusion and rotation. Comparison with experimental data is made by linking calculated diffusion coefficients to pulse field gradient nuclear magnetic resonance (PFG NMR) spectroscopy and rotational correlation times to relaxation measurements. NMR spectroscopy is chosen because experimentally it provides a convenient and non-invasive means for measuring molecular motion.[25–27]

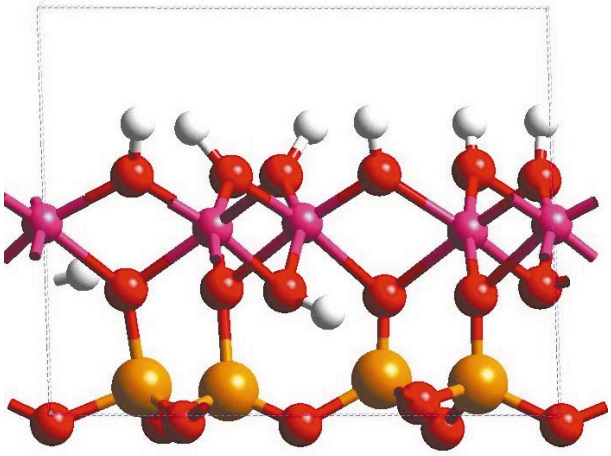

Fig. 1 Structure of kaolinite: O atoms are red, the tetrahedral Si atoms are yellow, octahedrally coordinated Al are pink, and H atoms are white. The "Al surface" is the top layer and the "Si surface" is the bottom layer.

2 Theoretical methods

2.1 Static simulations

Static simulations of the perfect lattice of bulk kaolinite yield the crystal structure and the lattice energy. In the static limit, the structure of the lattice is determined by the condition that it is in equilibrium, *i.e.*,

$$\partial E/\partial X_i = 0 \quad (1)$$

in which E is the static contribution to the internal energy, and the $\{X_i\}$ are the variables that define the structure. The $\{X_i\}$ consist of the three lattice vectors and the atomic positions in the unit cell.

For our atomistic simulation we assume that surfaces are planar. Irregularities such as steps, kinks and ledges, which are present on real surfaces, are omitted for the present treatment. For kaolinite the energy of the {001} basal surface was evaluated using a suitable supercell containing 425 atoms. The structure for amorphous silica was generated using a model defined in the Cerius[2] simulation package[28] and comprises SiO_2 and SiOH units with a ratio of 9 : 1 in the bulk. At the surface the ratio is closer to 3 : 1.

The success of any simulation relies on the accuracy and transferability of the short range interatomic potentials. As in a recent study of muscovite,[24] we have used a well established set of atomic charges and potentials developed by Collins and Catlow[29] and also incorporating the O–H potential added to this set by de Leeuw *et al.*[30] in their study of hydroxylated MgO surfaces.

2.2 Molecular dynamics simulations

Here we have used molecular dynamics (MD) simulations at constant volume and temperature (NVT) using the DLPOLY code.[31] The surfaces of the minerals considered here have a net dipole moment perpendicular to the surface (type III according to the Tasker classification[32]). To ensure that the periodic simulation cell had no net dipole moment, the cells contained either two kaolinite slabs, inverted with respect to each other, consisting of 425 atoms and 820 water molecules (25.81 Å × 26.70 Å × 77.00 Å), or two silica slabs in contact with 800 water molecules (28.50 Å × 28.50 Å × 80.00 Å). The interlayer separation between two kaolinite layers is ≈35–40 Å. The same interatomic potentials were used as for the static simulations, allowing all atoms within the clay to move. The charges and potentials for water were those of the TIP3P model.[31,33,34] Interactions between the water molecules and the mineral surface were calculated using the Lorentz–Berthelot geometric mixing rules. For those simulations also including ions in the water layer potentials for Na^+ and Cl^- potentials were extracted from the AMBER/OPLS force field.[31,34] Short range terms in the interaction potential were cut off at 8.0 Å, while long range Coulombic interactions are calculated using the Ewald technique.[35]

Water molecules (density 1 g cm^{-3}) were placed uniformly within the periodic cell. Dynamics simulations were carried out at 298 K for 100 ps. Time steps were set at 0.001 ps and a Berendsen thermostat[36] was used with a time step of 0.5 ps. Typically, 20 ps were used for equilibration runs, followed by production runs of 80 ps.

3 Results

3.1 Static simulations

Table 1 lists the experimental lattice parameters for bulk kaolinite, together with those calculated in the static limit. The largest discrepancy is 2.9% for b, which is reasonable considering our calculations relate to an idealised clay structure. The resulting surface energy, which is an average of the energies of the aluminium and silicon terminated surfaces of kaolinite (shown as the top and bottom layers in Fig. 1), is 48 mJ m^{-2}. This value is in surprisingly good agreement with values predicted experimentally using adsorption isotherm film pressures (34–103 mJ m^{-2}),[37] and contact angles of solutions on the kaolinite surface (35–96 mJ m^{-2}).[38]

3.2 Molecular dynamics simulations

Fig. 2(b) shows the simulated density profile of the centre of mass of water molecules in one dimension along an axis perpendicular to the clay surface. The scale is such that $-5.5 < z < 1.0$ and $23.0 < z < 29.5$ corresponds to the clay slabs. Significant structural ordering of the water at both clay surfaces may be observed in Fig. 2(b), as is clear by a comparison with Fig. 2(a), which shows the density profile for liquid water alone (density 0.98 g cm^{-3}). The extent of ordering of adsorbed water is in general agreement with experimental data for water at clay surfaces.[39,40] The appearance of ordering appears to be associated with the relatively ordered arrangement of oxygen atoms and OH groups at the clay surfaces. Fig. 3 shows a representative snapshot of the MD simulations carried out for Fig. 2(b), which reflects the alignment of the water molecules at the two surfaces. At the Si surface one or both water hydrogens may be involved in H-bonding to the oxygens of the silicate layer. At the Al surface all the atoms in

Table 1 Calculated and experimental lattice parameters for kaolinite

Lattice parameter	Simulation	Experiment
a/Å	5.135	5.155
b/Å	5.305	5.155
c/Å	7.321	7.405
α/°	75.05	75.14
β/°	83.13	84.12
γ/°	58.87	60.18

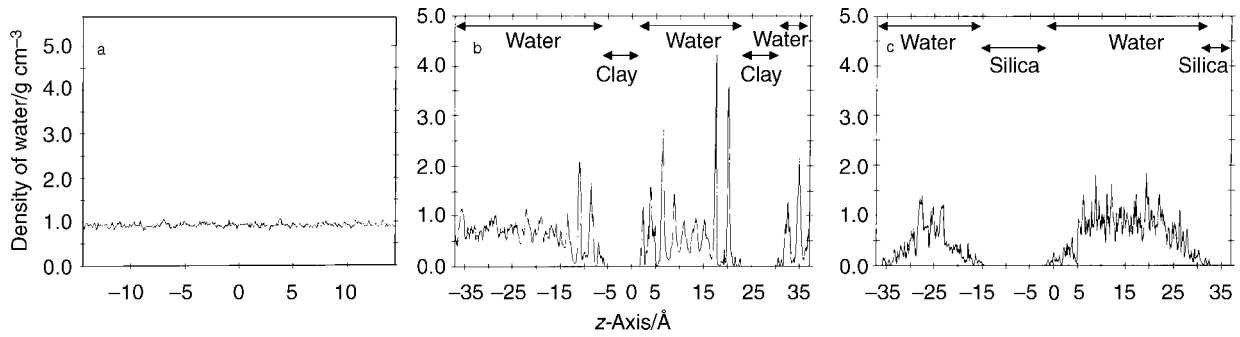

Fig. 2 (a) One-dimensional density profile of the centres of mass of water molecules in bulk water. (b) Density profile of the centres of mass of the water molecules along the z-axis (perpendicular to the surface) for kaolinite. (c) Density profile of the centres of mass of the water molecules along the z-axis (perpendicular to the surface) for amorphous silica.

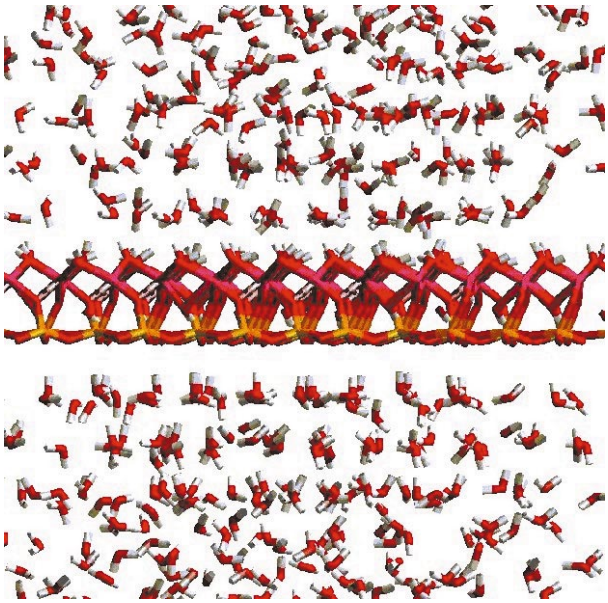

Fig. 3 Representative snapshot of the MD simulations carried out for Fig. 2(b).

the water molecules can take part in H-bonding to the surface OH groups. Unfortunately, molecular dynamics does not allow us to consider the effects of proton exchange at the surface.

The ordering at the kaolinite surface is striking when compared with similar calculations for the amorphous silica surface [Fig. 2(c)], which shows the ordering is substantially reduced relative to kaolinite. It is tempting to associate this disorder with the disorder at the silica surface; this is consistent with the snapshot in Fig. 4.

Figs. 5(a) and (b) show the change in the structural ordering of the water at the kaolinite and amorphous silica surfaces as the ionic strength of the solution is increased. In these calculations one Na^+ ion and a charge compensating Cl^- ion were introduced into the solvent. As might be expected the density profile at the kaolinite surface changes markedly, with a significant decrease in the peak intensity close to the surface [Fig. 5(a)], but there is still substantial ordering. There are far fewer changes above the amorphous silica surface [Fig. 5(b)]. Fig. 6(a) shows the density profile for kaolinite including a

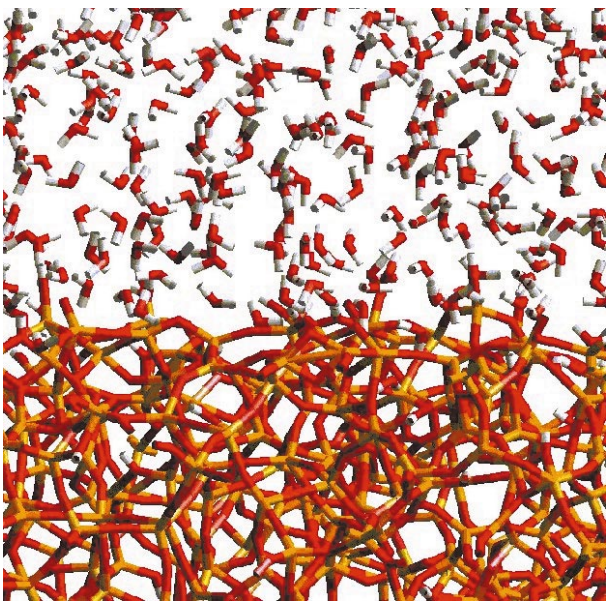

Fig. 4 Representative snapshot of the MD simulations carried out for Fig. 2(c). Atoms labelled as in Fig. 1.

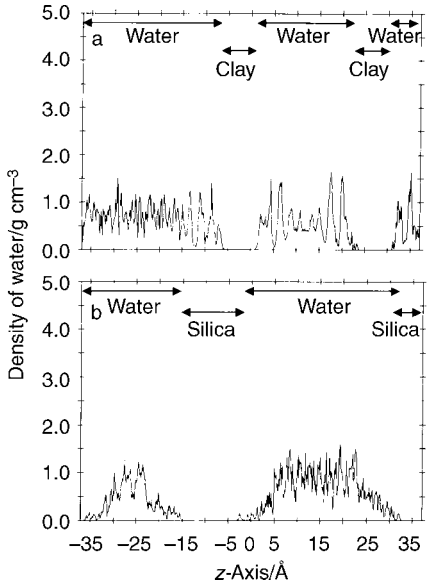

Fig. 5 (a) As Fig. 2(b), but with one Na^+ and one Cl^- added to the simulation box. (b) As Fig. 2(c), but with one Na^+ and one Cl^- added to the simulation box.

larger number of ions in the simulation box (10 Na^+, 10 Cl^-), equivalent to an ionic strength of $\sim$0.4 mol kg^{-1}. The ordering persists even at this much higher concentration, although the number of water molecules at the surface is significantly reduced. The reduced number of molecules at the surface may be accounted for by the displacement of water by Na^+. Fig. 7 shows a pictorial snapshot of one kaolinite surface during the simulation containing 10 Na^+ and 10 Cl^- ions. The water molecules have been removed for clarity; however the Na^+ ions can be seen to be adsorbing onto the surface, which has the effect of displacing the water.

3.3 Self-diffusion coefficients

Diffusion measurements for water were estimated by exploiting Einstein's relation:

$$6D = \lim_{t\to\infty} \frac{\mathrm{d}}{\mathrm{d}t} \langle |\boldsymbol{r}_i(t) - \boldsymbol{r}_i(0)|^2 \rangle \qquad (2)$$

where the diffusion coefficient of the water molecules, D, is related to the time averaged mean square displacement (Fig.

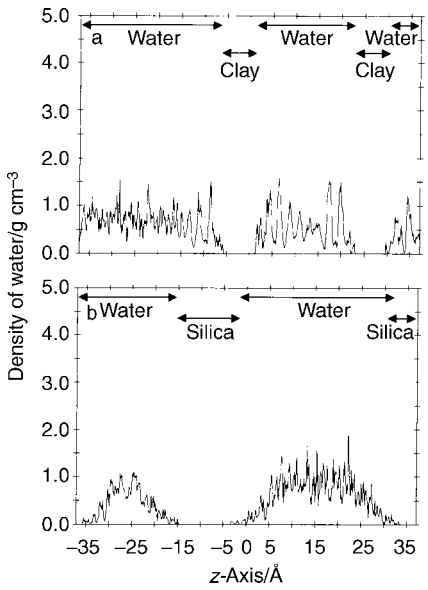

Fig. 6 (a) As Fig. 2(b), but with ten Na^+ and ten Cl^- added to the simulation box. (b) As Fig. 2(c), but with ten Na^+ and ten Cl^- added to the simulation box.

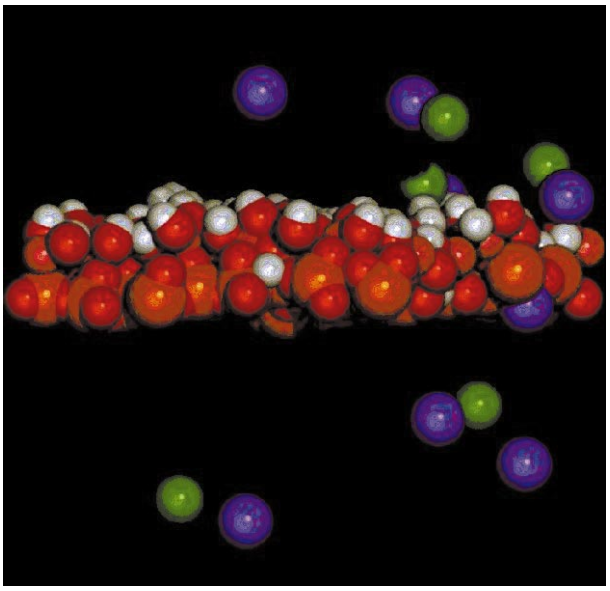

Fig. 7 A snapshot of the simulation of water, kaolinite and ten (Na^+, Cl^-). The picture shows the location of ions around one kaolinite surface. The Na^+ ions are purple while the Cl^- ions are green. Water molecules have been removed for clarity.

8). Calculated diffusion coefficients are given in Table 2. The value for bulk water, 3.9×10^{-9} m^2 s^{-1} (TIP3P), is in agreement with that from previous work[33] and is somewhat in excess of the experimental value[33] of 2.4×10^{-9} m^2 s^{-1}. This faster diffusion of simulated water is a reflection that the density of molecules (0.98 g cm^{-3}) in the periodic cell is slightly lower than that found experimentally (1.00 g cm^{-3}). For

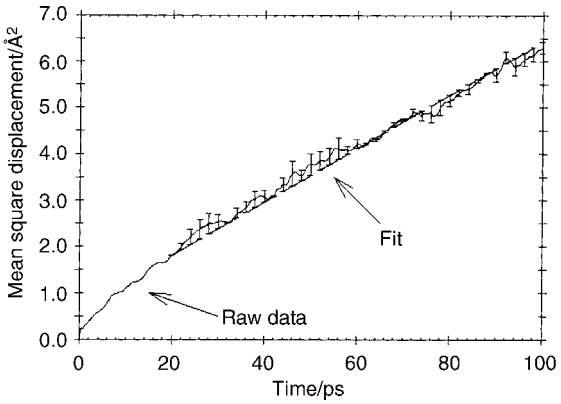

Fig. 8 An example of the mean square displacement data used to determine the diffusion coefficient for water. These data are taken for the simulation of water and kaolinite. Error bars are marked at 2 ps intervals.

Table 2 Average self-diffusion coefficients (D) of water in various environments

Model	Simulated diffusion coefficient/m^2 s^{-1}
TIP3P bulk water	3.9×10^{-9}
Water at the kaolinite interface	9.6×10^{-11}
Water at the kaolinite interface $+1(Na^+Cl^-)$	7.5×10^{-11}
Water at the kaolinite interface $+10(Na^+Cl^-)$	6.9×10^{-11}
Water at the silica surface	2.6×10^{-11}
Water at the silica surface $+1(Na^+Cl^-)$	2.7×10^{-11}
Water at the silica surface $+10(Na^+Cl^-)$	3.1×10^{-11}

both kaolinite and amorphous silica surfaces, the average diffusion coefficients for all water molecules in the simulation cell drop by over an order of magnitude, reflecting the marked ordering of the water molecules. Assuming that fast exchange of water between the bulk and surface regions occurs,[27] it would be expected that diffusion of water molecules in the surface region was even slower than the average value for the simulation box. Increasing the ionic strength of the solution has a much smaller effect on the average diffusion coefficients, for both kaolinite and silica, as shown by the remaining entries in Table 2. Diffusion in the z-direction (perpendicular to the surface) in the interfacial region is considerably slower than diffusion in the bulk phases.

3.4 Dynamics of reorientation

To consider the reorientational motion of water molecules, we use the approach of Impey, Madden and McDonald.[41] We calculate the time autocorrelation function of the second Legrendre polynomial P_2 of the angle subtended by the intramolecular H–H bond vector at time t with respect to its position at time $t = 0$:

$$C_2^{H-H}(t) = \langle P_2[\boldsymbol{e}^{H-H}(t) \cdot \boldsymbol{e}^{H-H}(0)] \rangle \quad (3)$$

$\boldsymbol{e}$ is a unit vector with the same direction as the H–H interatomic vector and $\langle\ \rangle$ represents the average over all molecules at time t.

The $C_2^{H-H}(t)$ function has a short range oscillatory part associated with the vibrational motion of each water molecule in a long-lived solvent "cage" and a long range slow decay associated with the breakup of the cage. In the exponential regime at large $t(>20$ ps) least squares fitting of $C_2^{H-H}(t)$ to the exponential function $A \exp(-t/t_c)$ (Fig. 9) allows us to determine the rotational correlation time, τ_c, given by At_c. Rotational correlation times are listed in Table 3.

As with the diffusion coefficients, the effect of the ordering imposed by the clay surface is clearly evident. Average corre-

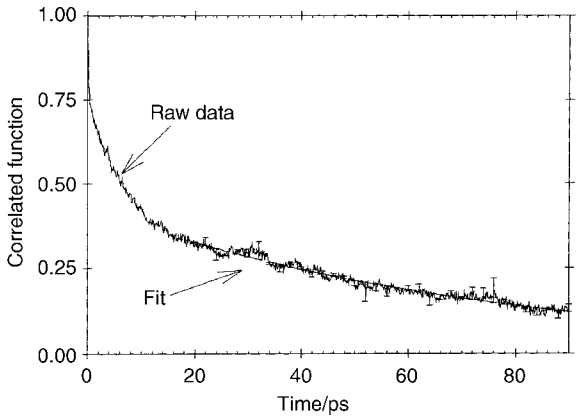

Fig. 9 An example of the $C_2^{H-H}(t)$ function calculated for water at the kaolinite surface. Error bars are labelled at 2 ps intervals.

Table 3 Average rotational correlation functions (τ_c) of water in various environments

Model	Rotational correlation function/ps
TIP3P bulk water	2.2
Water at the kaolinite interface	23.3
Water at the kaolinite interface $+1(Na^+Cl^-)$	33.5
Water at the kaolinite interface $+10(Na^+Cl^-)$	31.9
Water at the silica surface	85.1
Water at the silica surface $+1(Na^+Cl^-)$	95.5
Water at the silica surface $+10(Na^+Cl^-)$	81.0

lation times for all molecules in the periodic box increase by at least an order of magnitude compared with that of liquid water itself, a conclusion consistent with the work of Smirnov and Bougeard.[19] Increase in ionic strength appears to have only a relatively small effect.

3.5 Average NMR relaxation times

NMR relaxation times for water at the kaolinite surface are predicted using the approach of Carrington and McLachlan.[42] In this paper we restrict ourselves to a brief outline. Pure water can be described quantum mechanically as a particle with $I = 1$ since the total spin angular momentum is conserved during molecular tumbling. For $\omega^2\tau_c^2 \ll 1$, where ω is the angular velocity and τ_c is the rotational correlation coefficient, the relaxation time has two contributions, one from the rotation of the molecule (T_{1rot}) and one from the translation (T_{1trans}). Using perturbation theory, the relaxation or longitudinal magnetisation time, T_1, of the water molecule is then given by

$$\frac{1}{T_1} = \frac{1}{T_{1rot}} + \frac{1}{T_{1trans}} \tag{4}$$

The rotation of the molecule causes a magnetic dipole–dipole interaction between the protons in the molecule, which is a function of the distance r between the two dipoles. The relaxation rate, $(1/T_{1rot})$, varies linearly with the rotation correlation coefficient, τ_c:

$$\frac{1}{T_{1rot}} = \left(\frac{\mu_0}{4\pi}\right)^2 \frac{3}{2} \frac{\gamma_{1H}^4 \hbar^2 \tau_c}{r^6} \tag{5}$$

where μ_0 is the permeability constant and γ_{1H} is the gyromagnetic constant.

Water molecules diffusing past each other cause further intermolecular magnetic dipole–dipole interactions. These are a function of the concentration of spins, N, the average diffusion coefficient, D, and the distance of closest approach between the spins, b:

$$\frac{1}{T_{1trans}} = \left(\frac{\mu_0}{4\pi}\right)^2 \frac{\pi}{2} \frac{\gamma^4 \hbar^2 N}{Db} \tag{6}$$

We have taken $N = 6.75 \times 10^{28}$ m^{-3} and $b = 1.74$ Å, consistent with the size of the simulation box and the number of water molecules, and estimated average NMR relaxation times, T_1, from our simulation results. These are listed in Table 4.

3.6 NMR surface relaxation

Our values for T_1 are an average of both water molecules at the surface and water molecules in the bulk. Assuming a fast exchange limit[27] then expressions for the correlation time and relaxation time of water in the surface region can be defined using eqns. (7) and (8) respectively:

$$\tau_c = (1 - P_s)\tau_c + P_s\tau_c \tag{7}$$

$$\frac{1}{T_1} = \frac{(1 - P_s)}{T_{1b}} + \frac{P_s}{T_{1s}} \tag{8}$$

where P_s is equal to the fraction of protons in the surface environment and the subscripts b and s represent bulk and surface regions. Table 5 shows predicted values for rotational correlation and surface relaxation. The specific surface relaxation rate constant, R_{1sp}, quantified by

$$R_{1sp} = \frac{1}{T_{1s}} \tag{9}$$

may also be determined, and is calculated for each simulation in Table 5.

Table 4 Estimated average NMR relaxation times of water in various environments

Model	NMR relaxation time/s
TIP3P bulk water	6.39
Water at the kaolinite interface	0.37
Water at the kaolinite interface +1(Na^+Cl^-)	0.27
Water at the kaolinite interface +10(Na^+Cl^-)	0.26
Water at the silica surface	0.10
Water at the silica surface +1(Na^+Cl^-)	0.10
Water at the silica surface +10(Na^+Cl^-)	0.11

4 Discussion

Given the good agreement between the simulated lattice parameters for kaolinite and those observed experimentally, and the fair reproduction of the dynamic properties of water, we have a strong basis for assuming that the model we use is suitable for investigating the NMR relaxation times for water at mineral surfaces. Average values for the diffusion coefficients and correlation times allow us to evaluate average NMR relaxation times. From the simulations a substantial decrease in the average diffusion coefficient, an increase in correlation time and hence a decrease in relaxation time of the water is seen upon the introduction of both kaolinite and silica surfaces, in agreement with experimental observations. There would appear to be correlation between the change in magnitude of the diffusion coefficient and the change in magnitude of the rotational correlation time for each system in the 2-D region, implying that the motions are not completely independent.

The marked difference in the relaxation times for the kaolinite and silica may be attributed to the nature of the surface. Intuitively, the H-bonding which influences the increased structure at the kaolinite surface would be expected

Table 5 Estimated surface diffusion coefficients, rotational correlation times and NMR relaxation times of water in various environments

Model	Surface rotational correlation time/ps	NMR surface relaxation time/ms	NMR surface relaxation rate constant/s^{-1}
Water at the kaolinite interface	107.1	77.8	12.8
Water at the kaolinite interface +1(Na^+Cl^-)	186.3	42.7	23.4
Water at the kaolinite interface +10(Na^+Cl^-)	176.9	42.1	23.8
Water at the silica surface	520.3	17.3	57.8
Water at the silica surface +1(Na^+Cl^-)	585.3	16.9	59.1
Water at the silica surface +10(Na^+Cl^-)	494.7	15.3	65.3

to give lower values for the relaxation time. However this is not observed in the simulations. Instead we see lower values for the silica surface, which is a result of water molecules becoming trapped in the cage like amorphous silica surface and hence the effective surface area is larger. This reflects experimental results where precipitated silica surfaces are microporous and water inclusion in the surface is common.

The addition of ions to both the kaolinite and silica systems shows different trends. Increasing the ionic strength in the kaolinite system results in water molecules being displaced from the surface. The long range order of the water in the bulk is disturbed, as seen in the density profiles; however a high degree of structure remains at the surface, the driving forces of which are the kaolinite itself and the hydration shells around the ions. The silica surfaces appear less affected by ionic strength, which is reflected in both the values of T_1 and the density profiles. This is attributed to the lower fraction of OH groups at the surface, reducing the tendency for ions to adsorb and create local ordering.

Although our interest here lies chiefly in the variation of T_1 from system to system, the magnitude of T_1 for water is likely to be overestimated slightly. This can be accounted for because we cannot consider the exchange of protons at the surface. To avoid the effects of proton exchange one must consider a system where purely intramolecular forces dominate the surface relaxation. For example, deuterium NMR relaxation (spin $I = 1$) is not complicated by intermolecular interactions and cross-relaxation effects. The predominant relaxation mechanism is the time modulation of the essentially intramolecular quadrupole interaction.[43,44]

The ratio of the values for the NMR relaxation times in water[42] and at the silica surface (10^{-1} s) are in good agreement with that observed experimentally (10^{-2}–10^{-1} s).[45] Effects due to ionic strength are minor. For kaolinite there are no experimental data for comparison due to problems with uneven coagulation. We predict values of the same order as for silica.

5 Conclusions

Molecular dynamics simulations of water molecules at the surface of kaolinite, and of amorphous silica, have been carried out. In contrast to previous work, clay and silica atoms are *not* kept fixed at their crystallographic positions; all atoms are allowed to move. In both cases there is a marked decrease of the self-diffusion coefficient and increase in the rotational correlation time. We consider the effects of increasing the ionic strength of the water. Comparison with experimental data is made by linking calculated diffusion and rotational correlation times to available pulse field gradient nuclear magnetic resonance (PFG NMR) spectroscopy relaxation measurements.

Acknowledgements

We are grateful to Imerys for financial support. We also thank Dr. David Skuse, Dr. David Greenfield and Dr. Jonathan Phipps of Imerys for helpful discussions. Computational facilities were provided by an EPSRC grant, GR/M34799, and a grant from the UK Facility for Computational Chemistry.

References

1 B. J. Teppen, K. Rasmussen, P. M. Bertsch, D. M. Miller and L. Schafer, *J. Phys. Chem. B*, 1997, **101**, 1579.
2 B. J. Teppen, C. H. Yu, D. M. Miller and L. Schafer, *J. Comput. Chem.*, 1998, **19**, 144.
3 T. Undabeytia, S. Nir, G. Rytwo, E. Morillo and C. Maqueda, *Clays Clay Miner.*, 1998, **46**, 423.
4 N. T. Skipper, G. Sposito and F. R. C. Chang, *Clays Clay Miner.*, 1995, **43**, 294.
5 N. T. Skipper, *Min. Mag.*, 1998, **62**, 657.
6 N. T. Skipper, K. Refson and J. D. C. McConnell, *J. Chem. Phys.*, 1991, **94**, 7434.
7 D. E. Smith, *Langmuir*, 1998, **14**, 5959.
8 N. T. Skipper, F. R. C. Chang and G. Sposito, *Clays Clay Miner.*, 1995, **43**, 285.
9 H. C. Moog, T. Streck and H. K. Cammenga, *Soil Sci.*, 1998, **163**, 382.
10 S. Karborni, B. Smit, W. Heidug, J. Urai and E. van Oort, *Science*, 1996, **271**, 1102.
11 A. Delville, R. J. M. Pellenq and J. M. Caillol, *J. Chem. Phys.*, 1997, **106**, 7275.
12 A. Delville, *J. Phys. Chem.*, 1995, **99**, 2033.
13 F. R. C. Chang, N. T. Skipper and G. Sposito, *Langmuir*, 1995, **11**, 2734.
14 F. R. C. Chang, N. T. Skipper and G. Sposito, *Langmuir*, 1997, **13**, 2074.
15 F. R. C. Chang, N. T. Skipper and G. Sposito, *Langmuir*, 1998, **14**, 1201.
16 C. H. Bridgeman and N. T. Skipper, *J. Phys.: Condens. Matter*, 1997, **9**, 4081.
17 E. S. Boek, P. V. Coveney and N. T. Skipper, *Langmuir*, 1995, **11**, 4629.
18 E. S. Boek, P. V. Coveney and N. T. Skipper, *J. Am. Chem. Soc.*, 1995, **117**, 12608.
19 K. S. Smirnov and D. J. Bougeard, *J. Phys. Chem. B*, 1999, **103**, 5266.
20 D. L. Bish and R. B. Von Dreele, *Clays Clay Miner.*, 1989, **37**, 289.
21 R. A. Young and A. W. Hewat, *Clays Clay Miner.*, 1988, **36**, 225.
22 J. M. Adams, *Clays Clay Miner.*, 1983, **31**, 352.
23 A. C. Hess and V. R. Saunders, *J. Phys. Chem.*, 1992, **96**, 4367.
24 J. A. Purton, N. L. Allan and J. D. Blundy, *J. Mater. Chem.*, 1997, **7**, 1947.
25 N. Bloembergen, E. M. Purcell and R. V. Pound, *Phys. Rev.*, 1948, **74**, 679.
26 T. Cosgrove and P. C. Griffiths, *Colloids Surf. A*, 1994, **84**, 249.
27 G. P. van der Beek, M. A. Cohen Stuart and T. Cosgrove, *Langmuir*, 1991, **7**, 327.
28 Cerius 2, Molecular Simulations Inc., San Diego, 1998.
29 D. R. Collins and C. R. A. Catlow, *Am. Mineral.*, 1992, **77**, 1172.
30 N. H. de Leeuw, G. W. Watson and S. C. Parker, *J. Chem. Soc., Faraday Trans.*, 1996, **92**, 2081.
31 T. R. Forester and W. Smith, CCLRC, Daresbury Laboratory, Warrington, England, 1995.
32 P. W. Tasker, *Philos. Mag.*, 1979, **39**, 119.
33 W. L. Jorgensen, J. Chandrasekhar, J. D. Madura, R. W. Impey and M. L. Klein, *J. Chem. Phys.*, 1983, **79**, 926.
34 S. J. Weiner, P. A. Kollman, D. T. Nguyen and D. A. Case, *J. Comput. Chem.*, 1986, **7**, 230.
35 J. M. Ziman, *Principles of the Theory of Solids*, Cambridge University Press, Cambridge, 1964.
36 H. J. C. Berendsen, J. P. M. Postma, W. F. van Gunsteren, A. di Nola and J. R. Haak, *J. Chem. Phys.*, 1984, **81**, 3684.
37 E. Chibowski and P. Staszczuk, *Clays Clay Miner.*, 1988, **36**, 455.
38 B. Janczuk, E. M. H. Chibowski, T. Bialopiotrowicz and J. Stawinski, *Clays Clay Miner.*, 1989, **37**, 269.
39 R. E. Grim, *Clay Mineralogy*, McGraw-Hill, New York, 2nd edn., 1968.
40 A. Delville and M. Letellier, *Langmuir*, 1995, **11**, 1361.
41 R. W. Impey, P. A. Madden and I. R. McDonald, *Mol. Phys.*, 1982, **46**, 513.
42 A. Carrington and A. D. McLachlan, *Introduction to Magnetic Resonance*, Chapman and Hall, New York, 1980.
43 P. Roose, H. Bauwin and B. Halle, *J. Phys. Chem. B*, 1999, **103**, 5167.
44 A. Abragam, *Principles of Nuclear Magnetism*, Clarendon Press, Oxford, 1961.
45 H. Pfeifer, *NMR: Basic Princ. Prog.*, 1972, **7**, 55.